HHS Public Access

Author manuscript

Diabetologia. Author manuscript; available in PMC 2021 August 01.

Published in final edited form as:

Diabetologia. 2020 August ; 63(8): 1564–1575. doi:10.1007/s00125-020-05168-7.

Islet pericytes convert into profibrotic myofibroblasts in a mouse model of islet vascular fibrosis

Luciana Mateus Gonçalves[1,2], **Elizabeth Pereira**[1,3], **João Pedro Werneck de Castro**[1], **Ernesto Bernal-Mizrachi**[1,4], **Joana Almaça**[1]

[1]Division of Endocrinology, Diabetes and Metabolism, Department of Medicine, University of Miami Miller School of Medicine, Miami, FL 33136, USA

[2]Obesity and Comorbidities Research Center, Department of Structural and Functional Biology, Institute of Biology, University of Campinas, Campinas, SP, Brazil.

[3]Department of Physiology and Biophysics, Miller School of Medicine, University of Miami, Miami, USA,

[4]Miami VA Health Care System, Miami, Florida 33136, USA

Abstract

Aims/hypothesis—Islet vascular fibrosis may play an important role in the progression of type 2 diabetes, but there are no mouse models allowing detailed mechanistic studies to understand how a dysfunctional islet microvasculature contributes to diabetes pathogenesis. Here we report that the transgenic *AktTg* mouse, unlike other mouse strains, shows an increased deposition of extracellular matrix (ECM) proteins in perivascular regions, allowing us to study the cellular mechanisms that lead to islet vascular fibrosis.

Methods—Using immunohistochemistry, we labelled the islet microvasculature and ECM in pancreas sections of *AktTg* mice and human donors and performed lineage tracing to follow the fate of islet pericytes. We compared islet microvascular responses in living pancreas slices from wild-type and *AktTg* mice.

Results—We found that vascular pericytes proliferate extensively, convert into profibrotic myofibroblasts and substantially contribute to vascular fibrosis in the *AktTg* mouse model. The increased deposition of collagen I, fibronectin and periostin within the islet is associated with diminished islet perfusion as well as impaired capillary responses to noradrenaline (norepinephrine) and to high glucose in living pancreas slices.

Conclusions/interpretation—Our study thus illustrates how the *AktTg* mouse serves to elucidate a cellular mechanism in the development of islet vascular fibrosis, namely a change in

Corresponding author: Joana Almaça, Division of Endocrinology, Diabetes and Metabolism, Department of Medicine, University of Miami Miller School of Medicine, Miami, FL 33136, USA, jalmaca@med.miami.edu.

Authors' relationships and activities The authors declare that there are no relationships or activities that might bias, or be perceived to bias, their work.

Contribution statement JA and EBM designed the study; LMG, EP, JPWC and JA performed experiments; LMG and JA analysed data; JA and EBM wrote the manuscript. All authors revised the manuscript and approved its final version. JA is the guarantor of this work.

Data availability Data presented in this manuscript are available upon request from the authors.

pericyte phenotype that leads to vascular dysfunction. Because beta cells in the *AktTg* mouse are more numerous and larger, and secrete more insulin, in future studies we will test the role beta cell secretory products play in determining the phenotype of pericytes and other cells residing in the islet microenvironment under physiological and pathophysiological conditions.

Keywords

Extracellular matrix; Fibrosis; Hyperinsulinaemia; Microvasculature; Myofibroblast; Pancreatic islet; Pericyte

Introduction

Pancreatic islets are highly vascularised endocrine mini-organs that regulate glucose homeostasis [1]. Their dense network of blood vessels and extracellular matrix (ECM) are essential to maintain endocrine cell survival and function [2]. Islets in people with type 2 diabetes are characterised by vascular fibrosis consisting of an excessive deposition of ECM proteins around islet blood vessels [3]. Although it is not central to current models of diabetes pathogenesis [4], earlier studies suggested that islet vascular fibrosis plays an important role in the pathogenesis of type 2 diabetes [5]. Vascular fibrosis could lead to defective hormone secretion either by causing cytoarchitectural defects and reducing beta cell mass [6–10] or by compromising microvascular function, causing vascular leakage [11] and interfering with exchanges between endocrine cells and the blood [12, 13]. Little is known, however, about the specific cellular and molecular mechanisms that promote islet vascular fibrosis in type 2 diabetes. Unfortunately, there is a lack of adequate model organisms allowing detailed mechanistic studies to understand how a dysfunctional islet microvasculature contributes to diabetes pathogenesis.

The mouse is widely used to study islet biology and diabetes pathogenesis because it can be manipulated to establish causal relationships. However, important aspects of the microvasculature and the local extracellular microenvironment of the human islet are not modelled in the mouse. The human islet has fewer and shorter blood vessels, with smaller vessel diameters and reduced vessel branching than mouse islets [14, 15]. There are major differences in the composition of the basement membrane [16], including a dense accumulation of collagen around the microvasculature in the human islet [[17]; Fig. 1). A caveat to these comparisons is that they are made mostly to the C57BL/6 mouse, which may not be the best choice to study islet vascular biology and the local microenvironment. We searched for a mouse model for studying pathophysiological changes in the islet microvasculature and found the *AktTg* mouse: a transgenic mouse model of beta cell expansion, whose beta cell mass is significantly higher than in wild-type animals owing to enhanced beta cell hyperplasia and hypertrophy [18]. Importantly, islets from these mice showed an increased deposition of ECM proteins in perivascular regions, allowing us to study cellular mechanisms leading to vascular fibrosis in the islet.

Given their pluripotent and postnatal undifferentiated nature, vascular pericytes can adopt various phenotypes. For instance, pericytes can convert into myofibroblasts in fibrotic diseases in different tissues [19–23]. Pericytes at the islet border (endocrine–exocrine

interface) have been shown to adopt a myofibroblast-like appearance in rat models of type 2 diabetes and hypertension [13, 24]. We therefore hypothesised that, in the *AktTg* mouse, pericytes contribute to vascular fibrosis by becoming profibrotic myofibroblasts. We used cell lineage tracing to follow the fate of islet pericytes and assessed the functional consequences of the anatomical alterations of the islet microvasculature using living mouse pancreas slices.

Methods

Detailed descriptions of the experimental procedures can be found in the electronic supplementary material (ESM) Methods.

Mice

All the experiments were performed with 3–4 month old female and male mice, on a C57BL/6 background. *AktTg* mice were generated as previously described and bred in house [18]. All other mouse lines were from the Jackson Laboratory (USA). For lineage tracing experiments, we crossed male mice that expressed the fluorescent reporter tdTomato (*Rosa26*-tdTomato, stock no. 012567) with female mice that express Cre recombinase under the *Cspg4* promoter (NG2-Cre, stock no. 008533; note that *Cspg4* encodes neuron–glial antigen 2 [NG2], which is also known as chondroitin sulphate proteoglycan 4). Cre-positive tdTomato-positive female mice were crossed with *AktTg* male mice to yield NG2-tdTomato-*AktTg* mice. Mice harbouring a spontaneous mutation in the leptin receptor (*db/db* mice; stock no. 000697) were also used. To label proliferating cells, BrdU (1 mg/ml) was added to the drinking water for 21 days. All experiments were conducted according to protocols approved by the University of Miami Institutional Animal Care and Use Committee.

Organ donors

Human pancreas tissue sections were obtained from the Histology Core of the Diabetes Research Institute of the University of Miami. Information about human organ donors is included in ESM Table 1. Experiments were approved by the responsible ethics committee of the University of Miami.

Picrosirius red staining

Picrosirius red stain in combination with polarisation microscopy was used to visualise collagen in tissue sections [25]. Pancreatic sections (10 μm) from wild-type, *db/db* and *AktTg* mice and human donors were deparaffinised in xylene and rehydrated in ethanol series before incubation with picrosirius red solution (0.5g of Direct red 80 in 500 ml of saturated aqueous solution of picric acid) for 60 min. The sections were washed twice with acidified water (5 ml acetic acid (glacial) in 1 l water), dehydrated and mounted. Slides were observed under a microscope (BX41, Olympus, USA) equipped with polarised light and images analysed with ImageJ software (http://imagej.nih.gov/ij/). The density of picrosirius red staining was calculated by dividing the area of red-stained structures within the islet parenchyma by the islet area. Quantification was performed in a blind fashion.

Preparation of living pancreatic slices

Pancreatic slices (150 μm thickness) were prepared from wild-type and *AktTg* mice (3–4 months old) as previously described [26]. Slices were incubated in HEPES-buffered solution containing 3 mmol/l glucose. For blood vessel labelling, *Lycopersicon esculentum* lectin conjugated to DyLight 594 (DL-1177, Vector Labs, USA) was injected (75μg) in the tail vein 10 min before sacrificing.

Confocal imaging of living pancreatic slices

Living pancreatic slices of wild-type and *AktTg* mice were imaged on a Leica SP5 upright confocal microscope (Leica Microsystems, Germany) using a ×40 water immersion objective [26]. Slices were continuously perfused with HEPES-buffered solution containing 3 mmol/l glucose. DyLight 594-labelled tomato lectin was excited at 594 nm and emission detected at 610–650 nm. Backscatter light was collected upon excitation with the 633 nm laser. We recorded changes in blood vessel diameter induced by noradrenaline (norepinephrine) (20 μmol/l), basal glucose solution (3 mmol/l), or by high glucose (16 mmol/l). To estimate the percentage of the islet microvasculature that was functional, we used ImageJ to quantify, in maximal projections of the islet, the area labelled with the lectin and divided it by the total islet blood vessel area (immunostained with an antibody against CD31). Quantification of islet blood vessel diameter was done as previously described [26]. Briefly, in confocal images of the islet, we drew a straight line transversal to the blood vessel borders and used the ‘reslice’ z-function in ImageJ to generate a single image showing the changes in vessel diameter over time [27]. We drew another line on the resliced image and, using the ‘plot profile’ function, we determined the position of the pixels with the highest fluorescence intensity and considered these the vessel borders. Vessel diameter was calculated by subtracting these 2 position values. Only one islet was imaged in each slice.

Immunohistochemistry

In this study we used 3–4 month old wild-type and *AktTg* mice of both sexes (n = 3). Mice were perfused with 4% PFA and the pancreases collected in tubes containing 4% PFA. Small pieces of human pancreatic tissue were fixed overnight with 4% PFA. Tissues were cryoprotected in a sucrose gradient and frozen in optimal cutting temperature compound (OCT) before cryosectioning. Immunohistochemistry was performed as previously described [26] and antibodies used can be found in the ESM Methods. We used ImageJ to estimate in confocal planes the numbers of pericytes and endothelial cells by manually counting the number of nuclei surrounded by cytoplasmic NG2 or CD31 immunostaining, divided by the islet area and multiplied by a mean area of 10,000 μm^2. To determine vessel and ECM protein densities, in maximal projection images, we divided total immunostained area by the islet area (visualised with insulin staining). To determine colocalisation between tdTomato (red channel) and pericytes, myofibroblast markers and ECM proteins (green channel), we used the ImageJ plugin ‘intensity correlation analysis’ and calculated Mander’s colocalisation coefficients (M1 and M2). Quantifications were performed in a blind fashion.

Quantitative real-time PCR

Pancreatic islets were isolated from NG2-tdTomato wild-type mice (~7 months old) and viable tdTomato-positive and negative cells were FACS sorted from cell suspensions. Quantitative real-time PCR was performed as described in the ESM Methods to determine the expression of the following genes: *Rn18s*, *Cspg4* (which encodes NG2), *Acta2*, *Pdgfrb*.

Statistics

We used GraphPad Prism 5.0 and performed Student's *t* test, one-sample *t* test or one-way ANOVA followed by a Tukey's multiple comparison test. We considered statistical significance when $p < 0.05$. All data were assessed to ensure normal distribution and equal variance between groups. Throughout the manuscript we present data as mean ± SEM, unless otherwise stated in the figure legend.

Results

A mouse model of islet vascular fibrosis

The microvasculature of the human islet differs from that of the mouse islet [14, 15]. In particular, the human islet is characterised by an accumulation of collagen fibres around its blood vessels [16, 17]. When we used the picrosirius red dye to specifically label collagen in pancreas sections, we found that the human islet microvasculature was outlined by the red staining (Fig. 1). Strikingly, already at a young age (17 years), ~10% of the human islet area contained picrosirius red-labelled connective tissue, a percentage that did not significantly increase with age (Fig. 1a, e). The islet microvasculature of wild-type C57BL/6 mouse, by contrast, was not stained at all (Fig. 1b, f). There were picrosirius red-labelled structures outside the mouse islet (e.g. connective tissue around acini, ducts and major blood vessels; Fig. 1b). Older C57BL/6 mice and *db/db* mice also did not show signs of islet vascular fibrosis (Fig. 1c). When we inspected the pancreas of the *AktTg* mouse, however, we found that there was intense picrosirius red labelling within the islet parenchyma, that appeared mostly as bright yellow or orange fibres upon polarised light (Fig. 1d,f and ESM Fig. 1).

The *AktTg* mouse is a transgenic mouse model of beta cell expansion [18]. This mouse has increased Akt activity in beta cells due to the expression of a constitutively active Akt1 (PKB α) mutant under the control of the insulin gene promoter. Beta cell mass is significantly greater than in wild-type animals owing to enhanced beta cell proliferation and hypertrophy, yielding much higher fasting and fed plasma insulin levels and improved glucose tolerance, while maintaining normoglycaemia ([18], ESM Fig. 2). In this context of beta cell expansion, we not only detected abundant vascular fibrosis with picrosirius red in *AktTg* islets (Fig. 1d, f), but also found increased type I collagen and fibronectin immunostaining within the islet (Fig. 1g–j). Laminin density was not different between islets from wild-type C57BL/6 mice and those from *AktTg* mice. Perivascular regions in *AktTg* islets were further labelled for periostin, a myofibroblast marker and a secreted ECM protein that is involved in cellular adhesion and organisation of collagen [28] (Fig. 1h, j). Therefore, we took advantage of these changes and used the *AktTg* mouse to study pathophysiological mechanisms associated with islet vascular fibrosis.

Altered islet microvasculature in islets from *AktTg* mice

In view of the increased islet vascular fibrosis in the *AktTg* mouse model, we then examined the islet microvasculature and its cellular components: endothelial cells and pericytes. Pericytes were immunostained with two bona fide pericyte markers, NG2 and platelet-derived growth factor receptor-β (PDGFRβ) [26]. Endothelial cells were either labelled with a fluorescent lectin from *Lycopersicon esculentum* (Fig. 2a) or immunostained with an antibody against the endothelial cell marker CD31 (also known as platelet endothelial cell adhesion molecule [PECAM]; Fig. 2b). We determined major alterations of the islet capillary network and pericyte coverage in *AktTg* mice (Fig. 2). While in wild-type mice the islet capillary network was more dense than in the surrounding exocrine tissue ([29]; Fig. 2a,c), islets from *AktTg* mice exhibited fewer blood vessels (Fig. 2a,c). The typical tube morphology of capillaries made of a layer of endothelial cells covered with pericytes was disrupted in *AktTg* islets (Fig. 2b). Blood vessels in *AktTg* islets had significantly more pericytes and endothelial cells (Fig. 2b, d, e). Wild-type islets displayed a 1:3 ratio of pericytes:endothelial cells, consistent with our previously reported ratio in mouse pancreatic islets ([26]; Fig. 2f). In contrast, *AktTg* islets showed a higher pericyte:endothelial cell ratio (~ 1:2; Fig. 2f). The morphology of blood vessels in the acinar tissue surrounding islets of *AktTg* mice was conserved (Fig. 2a,b). These results indicate that in the *AktTg* mouse the increased fibrosis is associated with changes in the structure and composition of the islet microvasculature.

Pericytes are activated and proliferate in islets from *AktTg* mice

To assess the contribution of proliferation to the increase in endothelial cell and pericyte numbers, we performed BrdU experiments. Consistent with published data [18], higher beta cell proliferation was observed in *AktTg* transgenic mice (ESM Fig. 2). Interestingly, approximately 60% of NG2-positive islet pericytes incorporated BrdU in *AktTg* mice, suggesting that the increase in pericyte number in *AktTg* islets was due to increased proliferation (Fig. 3a, d). The percentage of proliferating NG2-positive pericytes in *AktTg* mice was significantly higher than that of all the other cell populations analysed (Fig.3d): insulin-positive beta cells, CD31-positive endothelial cells, α smooth muscle actin (αSMA)-positive cells (smooth muscle, myofibroblasts, pancreatic stellate cells; [30]), PDGFRβ-positive pericytes/fibroblasts (Fig. 3b, d). There were also more proliferating PDGFRβ-positive pericytes in *AktTg* than in wild-type mouse islets (Figs 2g, 3c–d and ESM Fig. 3).

We then assessed the magnitude of activation of critical pathways known to promote growth and proliferation: the Akt and mitogen-activated protein kinase (MAPK)/extracellular signal-regulated kinase (ERK) signalling pathways. We used antibodies that recognise phosphorylated (active) Akt (pAkt, Ser 473) and phospho-p44/42 MAPK (ERK1/2) (Thr 202/Tyr 204). While low levels of pAkt were detected in pancreatic sections from wild-type mice, strong pAkt immunoreactivity was observed in *AktTg* islets (ESM Fig. 4). In *AktTg* islets, pAkt was detected at higher levels in endocrine cells. pAkt fluorescence intensity was also significantly higher in pericytes from *AktTg* islets than in pericytes in wild-type islets. pERK fluorescence could be detected in endocrine and vascular cells in wild-type islets, but its intensity significantly decreased in endocrine cells while remaining high in pericytes in

islets from *AktTg* mice (ESM Fig. 4). Indeed, islet pericytes and exocrine tissue exhibited the highest levels of pERK immunoreactivity in pancreatic sections from *AktTg* mice.

A subset of pericytes in *AktTg* islets differentiates into myofibroblasts

Pericytes are critical for microvascular homeostasis but, owing to their pluripotent and undifferentiated nature, pericytes can differentiate into myofibroblasts in progressive fibrotic diseases [19–22]. Myofibroblasts are the major source of extracellular matrix proteins that accumulate in tissue fibrosis. To determine if islet pericytes contribute to vascular fibrosis in *AktTg* islets, we first used immunostaining to assess the localisation of pericytes in relation to those of the matrix proteins collagen type I and periostin (Fig. 4). Extracellular collagen type I deposits around the microvasculature in *AktTg* islets were always found in close association with NG2-labelled pericytes, whose cytoplasmic processes seemed to wrap and surround these ECM aggregates (Fig. 4b, c, e). Pericytes labelled for the myofibroblast marker periostin were found in close association with this ECM protein (Fig. 4d). These data suggest that islet pericytes could contribute to the pool of profibrotic myofibroblasts in *AktTg* mice. Interestingly, pericytes in islets in pancreas sections from young non-diabetic individuals also express periostin and associate closely with collagen type I (ESM Fig. 5).

To determine the potential contribution of the pericyte population to the pool of profibrotic myofibroblasts, we performed lineage tracing studies by crossing a fluorescent reporter tdTomato mouse to mice expressing Cre recombinase under the *Cspg4* promoter (NG2-tdTomato mice). In these mice, vascular smooth muscle cells and pericytes express the reporter in peripheral tissues such as pancreatic islets (Fig. 5e and ESM Fig. 6; [26]). To validate the specificity of our Cre model, we sorted tdTomato-positive cells from NG2-tdTomato mice. As an internal control, we also collected tdTomato-negative cells. tdTomato-positive cells were indeed pericytes as shown by the increased levels of pericyte genes *Cspg4* (which encodes NG2), *Pdgfrb* and *Acta2* (which encodes αSMA) in these cells compared with tdTomato-negative cells (ESM Fig. 6).

To study changes in the pericyte phenotype in the *AktTg* mouse, NG2-tdTomato mice were transferred to the *AktTg* background to yield NG2-tdTomato-*AktTg* mice. NG2-tdTomato-*AktTg* mice showed plasma insulin levels, hypercellularity of vascular cells (ESM Fig. 6) and excessive perivascular ECM deposition typical of the *AktTg* background. Approximately 90% of tdTomato-positive cells were NG2-positive or PDGFRβ-positive mural cells in wild-type and *AktTg* islets, further confirming the specificity of the NG2-Cre model (Fig. 5e and ESM Fig. 6). A subset of lineage-traced tdTomato-positive cells was also labelled for αSMA, fibronectin and collagen type I in both wild-type and *AktTg* mice (Fig. 5c, e). Within the lineage-traced population of pericytes in islets from *AktTg* mice we found significant increases in the incidence of fibronectin labelled cells as well as de novo expression of fibroblast markers vimentin and periostin (Fig. 5a, b, e). These results indicate that pericytes give rise to profibrotic myofibroblasts in *AktTg* islets.

Myofibroblasts are a heterogenous cell population with different cellular origins. Of the periostin- and αSMA-positive cell populations in the islets of *AktTg* mice, 69 ± 3% and 40 ± 3% were tdTomato-positive, respectively. These data suggest that a subset of islet myofibroblasts (~30–60%) may originate from cell populations other than pericytes, such as

pancreatic stellate cells [31]. Nevertheless, islet pericytes contribute a substantial fraction of islet myofibroblasts in *AktTg* mice.

Impaired vascular perfusion and microvessel responses in *AktTg* islets ex vivo

To examine the functional consequences of the changes in islet pericytes and ECM in the *AktTg* model, we adapted the pancreatic slice technique to examine in situ responses of the fibrotic microvessels in their native environment [26, 32]. In living pancreatic tissue slices, the different tissue components are preserved allowing the study of interactions between endocrine cells, vascular cells, fibroblasts and other cell compartments. To assess the functionality of the islet microvasculature, we labelled blood vessels with an intravenous injection of a fluorescent lectin from *Lycopersicon esculentum* (Fig. 6a). There was a ~60% reduction in perfusion of *AktTg* islet, calculated as the percentage of the islet blood vessel area that was labelled with the lectin (functional vasculature; Fig. 6b). We then assessed whether the abnormalities in perfusion were associated with impaired responses to known capillary vasodilators and vasoconstrictors. In line with our published results [26], a subset of capillaries in wild-type mouse islets constricted upon noradrenaline stimulation (20 μmol/l; approximately 30% decrease in diameter) and dilated upon beta cell stimulation with high glucose (16 mmol/l; approximately 15% increase in diameter; Fig. 6c–e). Noradrenaline also elicited a powerful constriction of the feeding arteriole in wild-type islets (Fig. 6d, dark grey trace). In contrast, capillaries in *AktTg* islets were neither responsive to the vasoconstrictor noradrenaline nor to high glucose (Fig. 6c–e). Lack of responses of *AktTg* islet capillaries was not due to poor tissue viability as endocrine cells in *AktTg* islets still responded to KCl depolarisation (ESM Fig. 7). These data indicate that phenotypical alterations of pericytes and increased ECM accumulation around *AktTg* islet capillaries impair microvascular function. Islet microvascular dysfunction could be the cause of impaired insulin secretion per beta cell unit of *AktTg* mice in response to glucose in vivo (ESM Fig. 2d, [33]).

Discussion

Our results show that the *AktTg* mouse had substantial alterations of the islet microvasculature and ECM. In particular, blood vessel density in *AktTg* islets was lower than in wild-type mouse islets and the number of pericytes increased 2.5-fold, yielding a higher pericyte:endothelial cell ratio. In addition, the density of different ECM proteins in perivascular regions was significantly greater in *AktTg* islets, and a subset of islet pericytes converted into myofibroblasts and participated in increased ECM synthesis in this transgenic mouse model.

Our lineage tracing data show that pericytes in the islet parenchyma are capable of differentiating into myofibroblasts and are actively involved in ECM synthesis, similar to their role in fibrotic diseases in different tissues [19–23]. Our results are in line with a previous study in a rat model of type 2 diabetes, the human islet amyloid polypeptide rat, where a pericyte synthesising fibrillar collagen was observed at the interface between the endocrine and exocrine pancreas [13]. Interestingly, only a subset (approximately 40%) of islet pericytes adopted a myofibroblast-like phenotype, consistent with the notion that

pericytes are a very heterogeneous cell population [34]. Future studies will focus on identifying the cellular and molecular mechanisms that promote the expansion and differentiation of individual subsets of pericytes. Differential interaction with resident macrophages or with other recruited immune cells could determine whether or not they adopt a profibrotic phenotype [35, 36].

Given the higher beta cell mass and secretory activity, it is likely that islet pericytes in *AktTg* mice are abnormally exposed to beta cell secretory products that could affect their phenotype. Insulin, for instance, is a potent mitogenic peptide that controls cellular growth, proliferation, differentiation and migration. Insulin has been shown to stimulate the proliferation and growth of endothelial cells and pericytes in the retina [37, 38]. In addition, insulin also stimulates the proliferation of pancreatic stellate cells and the production of ECM proteins through a robust and sustained activation of Akt/mammalian target of rapamycin (mTOR) [39] or angiotensin II type 2 signalling pathways [40]. In our study we observed activation of Akt and MAPK/ERK signalling pathways in pericytes in *AktTg* islets (ESM Fig. 4). Both pathways are downstream of the insulin receptor, suggesting that pericytes could indeed be responding to higher levels of insulin. Future studies will determine whether insulin receptor activation is involved in the phenotypical change of the subset of islet pericytes that converts into myofibroblasts.

Excessive beta cell secretory activity could affect pericytes and the ECM by additional indirect mechanisms. Several beta cell secretory products are highly proinflammatory and could potentially activate myofibroblasts [41, 42]. For instance, ATP that is co-released with insulin is a strong activator of islet and acinar macrophages [32]. In addition, vascular endothelial growth factor A (VEGFA) released by beta cells leads to endothelial cell proliferation, thickening of the basement membrane of islet blood vessels, progressive macrophage infiltration, and proinflammatory cytokine production [43]. The potentially inflammatory environment in *AktTg* islets could also activate other subpopulations of myofibroblasts not derived from pericytes, such as pancreatic stellate cells [44]. These myofibroblast-like cells are usually found in the exocrine pancreas but are also present in pancreatic islets and their numbers increase in type 2 diabetic rats [31].

Endocrine cells in pancreatic islets depend on their blood vessels for proper function, and defects in the islet microvasculature can lead to diabetic phenotypes [45] However, because longitudinal and interventional studies are not possible in human beings, it is not known what happens at this vascular niche during the progression of type 2 diabetes. For instance, excessive deposition of ECM proteins around islet blood vessels has been described as the most frequent lesion in the islets of people with type 2 diabetes [3, 5] but neither the causes nor the functional consequences of islet vascular fibrosis have been fully elucidated. It has been suggested that the excessive deposition of connective tissue in perivascular regions in the islets could compromise capillary responses and the exchanges between beta cells and the circulation resulting in defective hormone secretion [12, 13]. Here we show that changes in pericyte coverage and perivascular fibrosis in *AktTg* islets lower the percentage of functional microvasculature and impair capillary responses to noradrenaline and glucose. These alterations have functional consequences. Indeed, when corrected for the significant increase in beta cell mass in *AktTg* mice, in vivo insulin secretion in response to glucose is

impaired in transgenic animals (ESM Fig. 2d). Similar findings were previously reported by Tuttle and colleagues when they measured insulin secretion from in situ perfused pancreases of *AktTg* mice [33]. These data support a potential negative impact of islet vascular fibrosis and chronic microvascular dysfunction on beta cell function. However, how acute, dynamic changes of islet microvascular function and blood flow impact hormone secretion still remains to be determined.

It is now clear that the function of pericytes goes beyond their role as mural cells of the microcirculation. Given their location at the interface between the blood and the islet parenchyma, pericytes are in a unique position to coordinate changes in the microenvironment with islet blood flow and perfusion and, ultimately, modulate islet hormone secretion. Pericytes can directly control islet perfusion and blood vessel function by actively modulating islet capillary diameter [26], or indirectly, by acquiring a myofibroblast-like phenotype and contributing to ECM synthesis as we show here. Excessive perivascular accumulation of ECM can result in deranged architecture and islet cell death, as well as impair microvascular function, leading, ultimately, to islet dysfunction. Using the *AktTg* mouse model, we now can conduct studies aimed at elucidating the role of insulin or other beta cell secretory products in determining the number, phenotype and function of islet pericytes. Elucidating the crosstalk between pericytes and beta cells is necessary to fully understand the pathogenesis of islet adaptation in diabetes.

Supplementary Material

Refer to Web version on PubMed Central for supplementary material.

Acknowledgements

The authors thank R. Barro Soria and A. Caicedo for carefully reviewing the manuscript, K. Johnson for histological work, J. Camperio and M. Canales for data quantification, and O. Umland for helping with FACS sorting pericytes (University of Miami).

Funding This work was funded by NIH grants K01DK111757 (JA), R01DK073716 (EBM) and DK084236 (EBM), as well as by the NIDDK-supported Human Islet Research Network (HIRN, RRID:SCR_014393; https://hirnetwork.org; UC4 DK104162, New Investigator Pilot Award to JA).

Abbreviations:

αSMA	α Smooth muscle actin
AktTg	Transgenic mice expressing constitutively active Akt1 in beta cells
ECM	Extracellular matrix
ERK	Extracellular signal-regulated kinase
MAPK	Mitogen-activated protein kinase
NG2	Neuron–glial antigen 2
PDGFRβ	Platelet-derived growth factor receptor-β
PECAM	Platelet endothelial cell adhesion molecule

References

[1]. Brunicardi FC, Stagner J, Bonner-Weir S, et al. (1996) Microcirculation of the islets of Langerhans. Long Beach Veterans Administration Regional Medical Education Center Symposium. Diabetes 45(4): 385–392 [PubMed: 8603757]

[2]. Nikolova G, Jabs N, Konstantinova I, et al. (2006) The vascular basement membrane: a niche for insulin gene expression and β cell proliferation. Developmental cell 10(3): 397–405. 10.1016/j.devcel.2006.01.015 [PubMed: 16516842]

[3]. Gepts W (1957) [Contribution to the morphological study of the islands of Langerhans in diabetes; study of the quantitative variations of the different insular constituents]. Annales de la Societe royale des sciences medicales et naturelles de Bruxelles 10(1): 5–108 [article in french] [PubMed: 13425197]

[4]. Halban PA, Polonsky KS, Bowden DW, et al. (2014) β-cell failure in type 2 diabetes: postulated mechanisms and prospects for prevention and treatment. Diabetes care 37(6): 1751–1758. 10.2337/dc14-0396 [PubMed: 24812433]

[5]. Gepts W, Lecompte PM (1981) The pancreatic islets in diabetes. The American journal of medicine 70(1): 105–115 [PubMed: 7006384]

[6]. Portha B, Lacraz G, Kergoat M, et al. (2009) The GK rat beta-cell: a prototype for the diseased human beta-cell in type 2 diabetes? Molecular and cellular endocrinology 297(1–2): 73–85. 10.1016/j.mce.2008.06.013 [PubMed: 18640239]

[7]. Ko SH, Kwon HS, Kim SR, et al. (2004) Ramipril treatment suppresses islet fibrosis in Otsuka Long-Evans Tokushima fatty rats. Biochemical and biophysical research communications 316(1): 114–122. 10.1016/j.bbrc.2004.02.023 [PubMed: 15003519]

[8]. Movassat J, Saulnier C, Serradas P, Portha B (1997) Impaired development of pancreatic beta-cell mass is a primary event during the progression to diabetes in the GK rat. Diabetologia 40(8): 916–925. 10.1007/s001250050768 [PubMed: 9267986]

[9]. Shima K, Shi K, Sano T, Iwami T, Mizuno A, Noma Y (1993) Is exercise training effective in preventing diabetes mellitus in the Otsuka-Long-Evans-Tokushima fatty rat, a model of spontaneous non insulin-dependent diabetes mellitus? Metabolism: clinical and experimental 42(8): 971–977. 10.1016/0026-0495(93)90009-d [PubMed: 8345821]

[10]. Mizuno A, Noma Y, Kuwajima M, Murakami T, Zhu M, Shima K (1999) Changes in islet capillary angioarchitecture coincide with impaired B-cell function but not with insulin resistance in male Otsuka-Long-Evans-Tokushima fatty rats: dimorphism of the diabetic phenotype at an advanced age. Metabolism: clinical and experimental 48(4): 477–483 [PubMed: 10206441]

[11]. Heydinger DK, Lacy PE (1974) Islet cell changes in the rat following injection of homogenized islets. Diabetes 23(7): 579–582. 10.2337/diab.23.7.579 [PubMed: 4601450]

[12]. Gepts W (1981) Islet changes in human diabetes In Cooperstein SJ, Watkins D (eds) The islet of Langerhans: biochemistry, physiology and pathology. Academic Press, Cambridge MA pp 321–356.

[13]. Hayden MR, Karuparthi PR, Habibi J, et al. (2008) Ultrastructure of islet microcirculation, pericytes and the islet exocrine interface in the HIP rat model of diabetes. Experimental biology and medicine (Maywood, NJ) 233(9): 1109–1123. 10.3181/0709-rm-251

[14]. Brissova M, Shostak A, Fligner CL, et al. (2015) Human Islets Have Fewer Blood Vessels than Mouse Islets and the Density of Islet Vascular Structures Is Increased in Type 2 Diabetes. The journal of histochemistry and cytochemistry 63(8): 637–645. 10.1369/0022155415573324 [PubMed: 26216139]

[15]. Cohrs CM, Chen C, Jahn SR, et al. (2017) Vessel Network Architecture of Adult Human Islets Promotes Distinct Cell-Cell Interactions In Situ and Is Altered After Transplantation. Endocrinology 158(5): 1373–1385. 10.1210/en.2016-1184 [PubMed: 28324008]

[16]. Virtanen I, Banerjee M, Palgi J, et al. (2008) Blood vessels of human islets of Langerhans are surrounded by a double basement membrane. Diabetologia 51(7): 1181–1191. 10.1007/s00125-008-0997-9 [PubMed: 18438639]

[17]. Van Deijnen JH, Van Suylichem PT, Wolters GH, Van Schilfgaarde R (1994) Distribution of collagens type I, type III and type V in the pancreas of rat, dog, pig and man. Cell and tissue research 277(1): 115–121. 10.1007/bf00303087 [PubMed: 8055531]

[18]. Bernal-Mizrachi E, Wen W, Stahlhut S, Welling CM, Permutt MA (2001) Islet β cell expression of constitutively active Akt1/PKBα induces striking hypertrophy, hyperplasia, and hyperinsulinemia. The Journal of clinical investigation 108(11): 1631–1638. 10.1172/jci13785 [PubMed: 11733558]

[19]. Dulauroy S, Di Carlo SE, Langa F, Eberl G, Peduto L (2012) Lineage tracing and genetic ablation of ADAM12^{+} perivascular cells identify a major source of profibrotic cells during acute tissue injury. Nature medicine 18(8): 1262–1270. 10.1038/nm.2848

[20]. Goritz C, Dias DO, Tomilin N, Barbacid M, Shupliakov O, Frisen J (2011) A pericyte origin of spinal cord scar tissue. Science 333(6039): 238–242. 10.1126/science.1203165 [PubMed: 21737741]

[21]. Humphreys BD, Lin SL, Kobayashi A, et al. (2010) Fate tracing reveals the pericyte and not epithelial origin of myofibroblasts in kidney fibrosis. The American journal of pathology 176(1): 85–97. 10.2353/ajpath.2010.090517 [PubMed: 20008127]

[22]. Lin SL, Kisseleva T, Brenner DA, Duffield JS (2008) Pericytes and perivascular fibroblasts are the primary source of collagen-producing cells in obstructive fibrosis of the kidney. The American journal of pathology 173(6): 1617–1627. 10.2353/ajpath.2008.080433 [PubMed: 19008372]

[23]. Schrimpf C, Xin C, Campanholle G, et al. (2012) Pericyte TIMP3 and ADAMTS1 modulate vascular stability after kidney injury. Journal of the American Society of Nephrology 23(5): 868–883. 10.1681/asn.2011080851 [PubMed: 22383695]

[24]. Hayden MR, Karuparthi PR, Habibi J, et al. (2007) Ultrastructural islet study of early fibrosis in the Ren2 rat model of hypertension. Emerging role of the islet pancreatic pericyte-stellate cell. Journal of the pancreas 8(6): 725–738 [PubMed: 17993725]

[25]. Junqueira LC, Bignolas G, Brentani RR (1979) Picrosirius staining plus polarization microscopy, a specific method for collagen detection in tissue sections. The Histochemical journal 11(4): 447–455. 10.1007/bf01002772 [PubMed: 91593]

[26]. Almaca J, Weitz J, Rodriguez-Diaz R, Pereira E, Caicedo A (2018) The Pericyte of the Pancreatic Islet Regulates Capillary Diameter and Local Blood Flow. Cell metabolism 27(3): 630–644 e634. 10.1016/j.cmet.2018.02.016 [PubMed: 29514070]

[27]. Fischer MJ, Uchida S, Messlinger K (2010) Measurement of meningeal blood vessel diameter in vivo with a plug-in for ImageJ. Microvascular research 80(2): 258–266. 10.1016/j.mvr.2010.04.004 [PubMed: 20406650]

[28]. Kanisicak O, Khalil H, Ivey MJ, et al. (2016) Genetic lineage tracing defines myofibroblast origin and function in the injured heart. Nature communications 7: 12260 10.1038/ncomms12260

[29]. Henderson JR, Moss MC (1985) A morphometric study of the endocrine and exocrine capillaries of the pancreas. Quarterly journal of experimental physiology 70(3): 347–356 [PubMed: 3898188]

[30]. Bachem MG, Schneider E, Gross H, et al. (1998) Identification, culture, and characterization of pancreatic stellate cells in rats and humans. Gastroenterology 115(2): 421–432 [PubMed: 9679048]

[31]. Lee E, Ryu GR, Ko SH, Ahn YB, Song KH (2017) A role of pancreatic stellate cells in islet fibrosis and β-cell dysfunction in type 2 diabetes mellitus. Biochemical and biophysical research communications 485(2): 328–334. 10.1016/j.bbrc.2017.02.082 [PubMed: 28232184]

[32]. Weitz JR, Makhmutova M, Almaca J, et al. (2018) Mouse pancreatic islet macrophages use locally released ATP to monitor beta cell activity. Diabetologia 61(1): 182–192. 10.1007/s00125-017-4416-y [PubMed: 28884198]

[33]. Tuttle RL, Gill NS, Pugh W, et al. (2001) Regulation of pancreatic β-cell growth and survival by the serine/threonine protein kinase Akt1/PKBα. Nature medicine 7(10): 1133–1137. 10.1038/nm1001-1133

[34]. Shepro D, Morel NM (1993) Pericyte physiology. FASEB journal : official publication of the Federation of American Societies for Experimental Biology 7(11): 1031–1038 [PubMed: 8370472]

[35]. Koyama Y, Brenner DA (2017) Liver inflammation and fibrosis. The Journal of clinical investigation 127(1): 55–64. 10.1172/jci88881 [PubMed: 28045404]

[36]. Shook BA, Wasko RR, Rivera-Gonzalez GC, et al. (2018) Myofibroblast proliferation and heterogeneity are supported by macrophages during skin repair. Science (New York, NY) 362(6417). 10.1126/science.aar2971

[37]. King GL, Buzney SM, Kahn CR, et al. (1983) Differential responsiveness to insulin of endothelial and support cells from micro- and macrovessels. The Journal of clinical investigation 71(4): 974–979. 10.1172/jci110852 [PubMed: 6339562]

[38]. King GL, Goodman AD, Buzney S, Moses A, Kahn CR (1985) Receptors and growth-promoting effects of insulin and insulinlike growth factors on cells from bovine retinal capillaries and aorta. The Journal of clinical investigation 75(3): 1028–1036. 10.1172/jci111764 [PubMed: 2984251]

[39]. Yang J, Waldron RT, Su HY, et al. (2016) Insulin promotes proliferation and fibrosing responses in activated pancreatic stellate cells. American journal of physiology Gastrointestinal and liver physiology 311(4): G675–G687. 10.1152/ajpgi.00251.2016 [PubMed: 27609771]

[40]. Kim JW, Ko SH, Cho JH, et al. (2008) Loss of beta-cells with fibrotic islet destruction in type 2 diabetes mellitus. Frontiers in bioscience : a journal and virtual library 13: 6022–6033. 10.2741/3133 [PubMed: 18508639]

[41]. Donath MY, Boni-Schnetzler M, Ellingsgaard H, Ehses JA (2009) Islet inflammation impairs the pancreatic β-cell in type 2 diabetes. Physiology (Bethesda, Md) 24: 325–331. 10.1152/physiol.00032.2009

[42]. Wynn TA (2008) Cellular and molecular mechanisms of fibrosis. The Journal of pathology 214(2): 199–210. 10.1002/path.2277 [PubMed: 18161745]

[43]. Agudo J, Ayuso E, Jimenez V, et al. (2012) Vascular endothelial growth factor-mediated islet hypervascularization and inflammation contribute to progressive reduction of β-cell mass. Diabetes 61(11): 2851–2861. 10.2337/db12-0134 [PubMed: 22961079]

[44]. Erkan M, Adler G, Apte MV, et al. (2012) StellaTUM: current consensus and discussion on pancreatic stellate cell research. Gut 61(2): 172–178. 10.1136/gutjnl-2011-301220 [PubMed: 22115911]

[45]. Richards OC, Raines SM, Attie AD (2010) The role of blood vessels, endothelial cells, and vascular pericytes in insulin secretion and peripheral insulin action. Endocrine reviews 31(3): 343–363. 10.1210/er.2009-0035 [PubMed: 20164242]

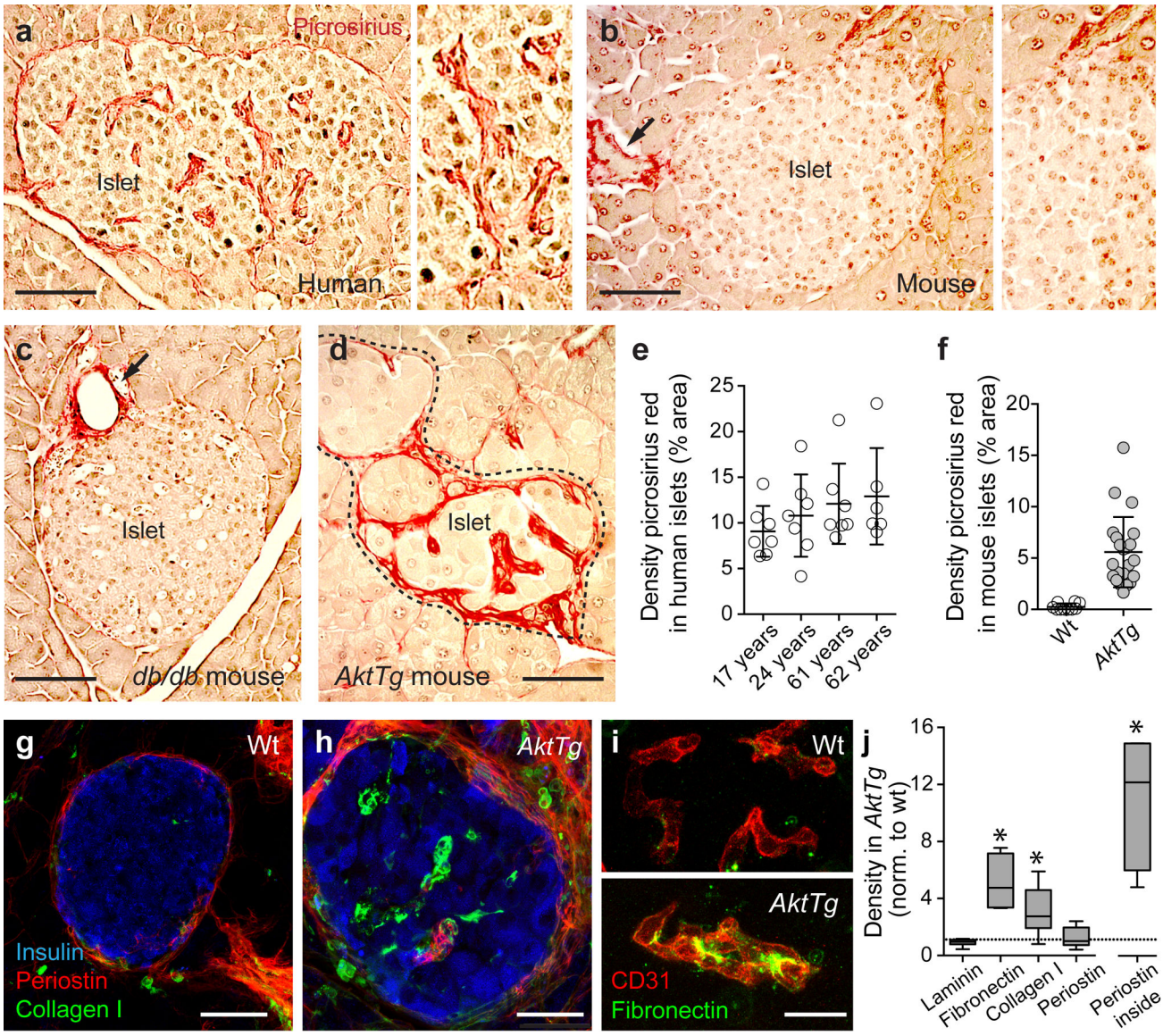

Fig. 1.

Perivascular accumulation of ECM in the *AktTg* transgenic mouse. (**a**–**d**) Representative images of islets in the pancreas of a non-diabetic human donor (17 years old; **a**), a C57BL/6 wild-type mouse (**b**), a *db/db* mouse (**c**) and an *AktTg* mouse (**d**), stained with the histology dye picrosirius red (red), which specifically stains collagens in tissue sections [25]. When visualised with polarised light, collagen fibres had a bright yellow or orange colour, suggesting it was mostly collagen type I (ESM Fig. 1). Young (3–4 months old) C57BL/6 wild-type, *db/db* and *AktTg* mice were used. (**e**) Quantification of the area labelled with picrosirius red divided by the total islet area (shown as %; mean ± SD) in islets in pancreatic sections from non-diabetic human donors with different ages; each data point is an islet. (**f**) Quantification of the area labelled with picrosirius red in wild-type (WT) and *AktTg* islets divided by the total islet area (shown as %; mean ± SD; n=3–5 islets/mouse, 3 mice per genotype). (**g**, **h**) Representative maximal projections of confocal images of islets from

C57BL/6 wild-type mouse and *AktTg* mouse (3 months old) immunostained for insulin (blue), collagen type I (green) and periostin (red). Collagen I and periostin can be visualised in the *AktTg* islet parenchyma. (**i**) Representative maximal projections of confocal images of blood vessels in islets from wild-type and *AktTg* mice immunostained for CD31 (PECAM, endothelial cell marker, red) and fibronectin (green). (**j**) Box and whisker plots showing the quantification of the islet area immunostained with antibodies against extracellular matrix proteins laminin, fibronectin, collagen type I and periostin divided by the total islet area, normalised (norm.) to the density of the same proteins in wild-type islets. 'Periostin inside' is the density of periostin within the islet parenchyma, i.e. excluding the interface between endocrine and exocrine compartments (capsule). *$p<0.05$ (one-sample *t* test using as theoretical mean the value of 1, indicated with the horizontal dashed line; $n=3–5$ islets/mouse, 3 mice per genotype). Scale bars, 50 μm (**a**–**d**), 20 μm (**g**, **h**) and 10 μm (**i**)

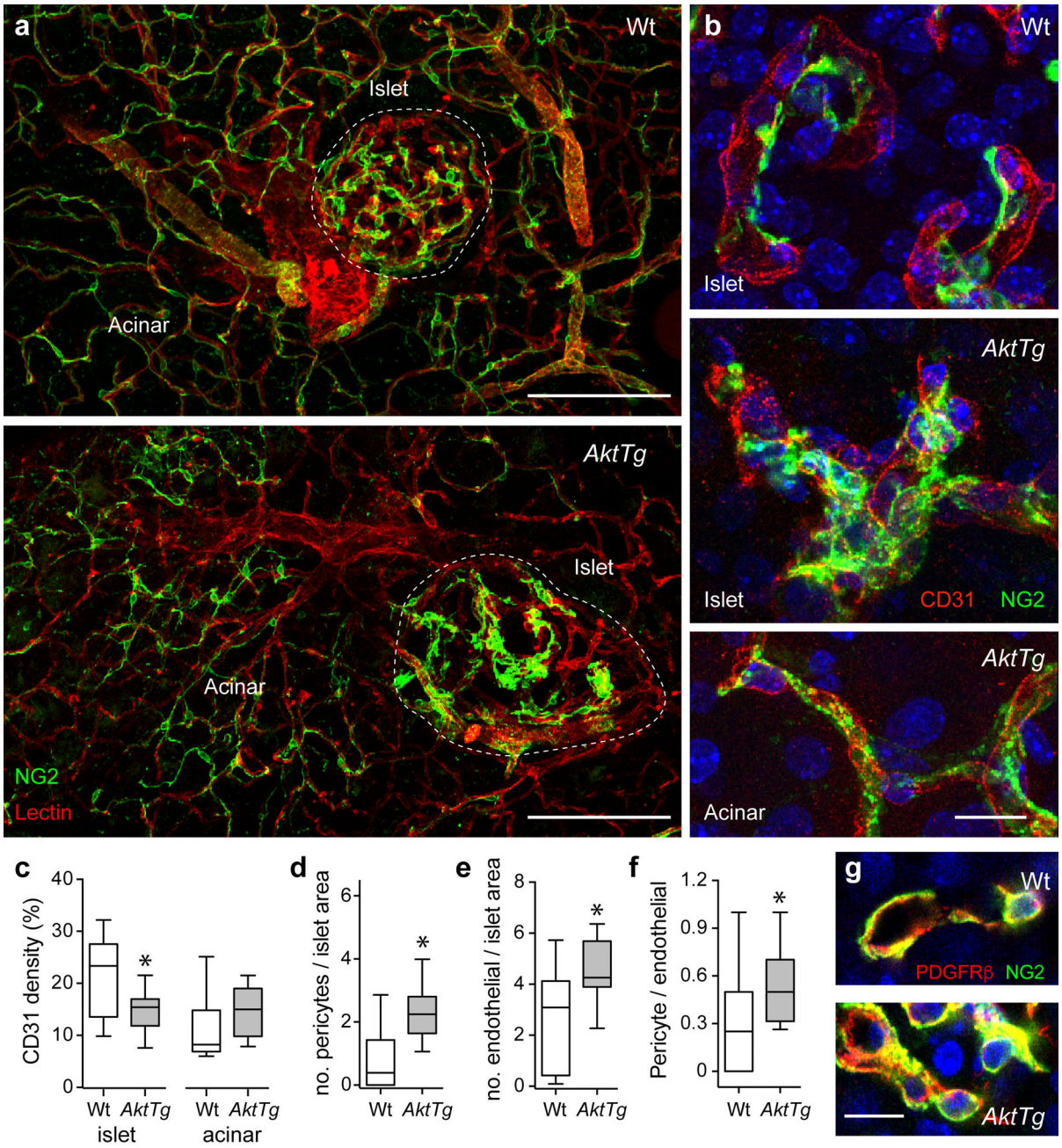

Fig. 2.

Altered islet microvasculature in islets from *AktTg* mice. (**a**) Representative maximal projections of confocal images of pancreases from C57BL/6 wild-type (WT) and *AktTg* mice showing blood vessels covered with pericytes. Blood vessels were labelled with a fluorescent lectin from *Lycopersicon esculentum* (red) and pericytes immunostained for NG2 (green). Increased pericyte coverage of *AktTg* islet capillaries is visible. Pericyte coverage of blood vessels in the acinar tissue in *AktTg* mice is apparently similar to that of wild-type acinar tissue. (**b**) Representative maximal projections of confocal images of blood vessels in islets from wild-type and *AktTg* mice showing pericytes and endothelial cells

immunostained, respectively, for NG2 (green) and for CD31 (PECAM, red). Cell nuclei were labelled with DAPI (blue). Pericytes nicely cover capillaries in wild-type islets but their coverage is increased in *AktTg* islets. Pericytes and capillaries in the acinar tissue of *AktTg* mice are not different from wild-type acinar vessels. (**c**) Quantification of the area covered with blood vessels (immunostained with an anti-CD31 antibody) in islets and surrounding acinar tissue in wild-type and *AktTg* pancreases, divided by the total area (shown as %). *$p<0.05$ (unpaired *t* test; $n=3$–5 islets/mouse, 3 mice per genotype). (**d**, **e**) Quantification of the total number of (**d**) NG2-labelled pericytes, or (**e**) CD31 labelled endothelial cells in confocal sections of islets from wild-type and *AktTg* mice, divided by the islet area and multiplied by a mean islet area of 10,000 μm^2. *$p<0.05$ (unpaired *t* test; $n=3$ confocal planes/islet, 5 islets/mouse, 3 mice per genotype). (**f**) Quantification of the ratio of pericyte number to endothelial cell number in confocal sections of wild-type and *AktTg* islets. *$p<0.05$ (unpaired *t* test; $n=3$ confocal planes/islet, 5 islets/mouse, 3 mice per genotype). (**g**) Representative maximal projections of confocal images of pericytes in wild-type and *AktTg* islets showing pericytes immunostained for NG2 (green) and PDGFRβ (red). Increased number of pericytes are present in *AktTg* islets. Scale bars, 100 μm (**a**) and 10 μm (**b**, **g**)

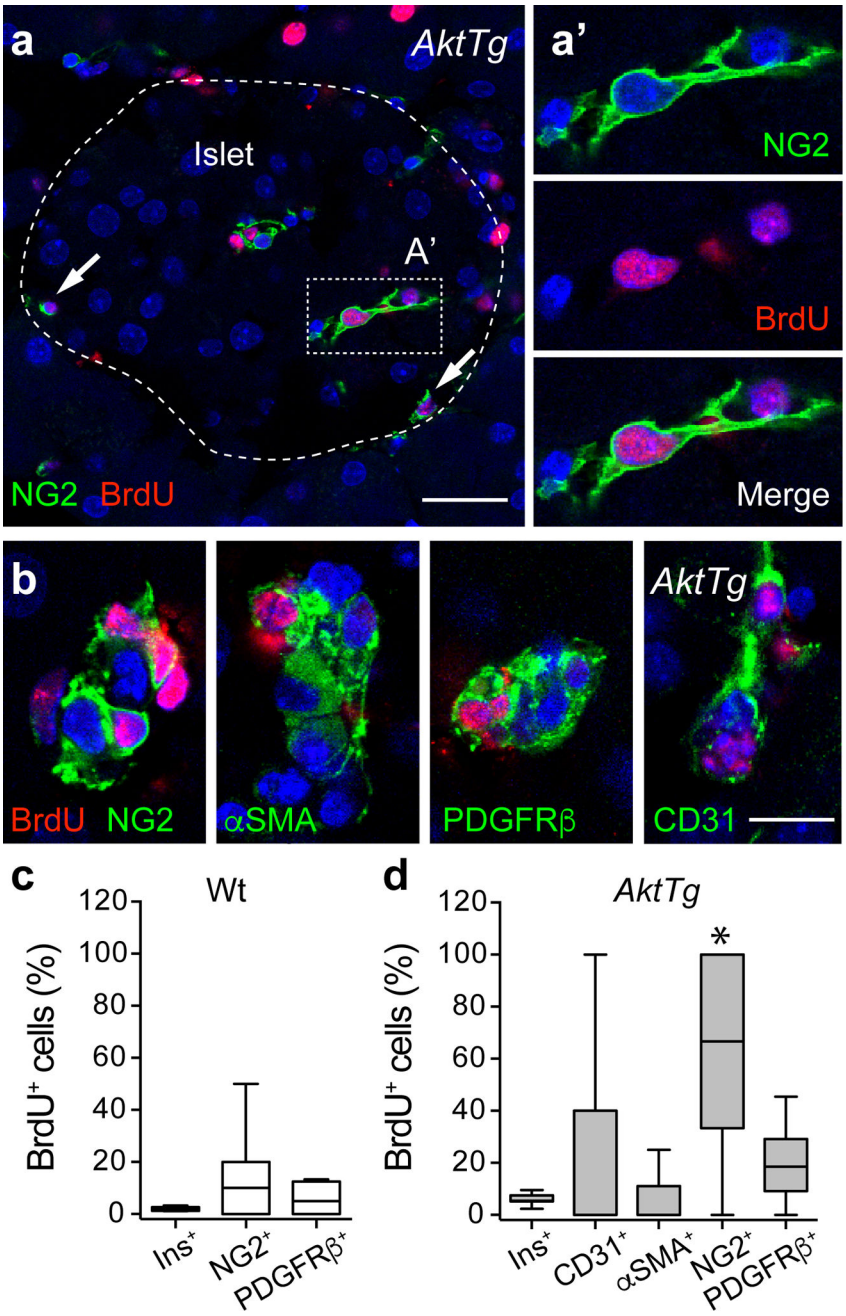

Fig. 3.

Increased pericyte proliferation in islets from *AktTg* mice. (**a**) Representative confocal image of an *AktTg* islet immunostained for NG2 (pericytes, green) and BrdU (red). The arrows indicate proliferating pericytes (BrdU-positive); the dashed line shows the islet border. (**a′**) Zoomed image of the region within the dashed rectangle shown in (**a**) of a pericyte that incorporated BrdU. (**b**) Representative confocal images of blood vessels within *AktTg* islets immunostained for BrdU (red) and NG2, αSMA, PDGFRβ or CD31 (green). Images of entire islets are shown in ESM Fig. 3. (**c**, **d**) Quantification of the percentage of insulin-positive beta cells (Ins^+), NG2-positive pericytes and PDGFRβ-positive pericytes/

fibroblasts that incorporated BrdU in wild-type (**c**) and *AktTg* islets (**d**). We also determined the percentage of proliferating CD31-positive endothelial cells and αSMA-positive mural cells/myofibroblasts in *AktTg* islets. The percentage of $NG2^{+}BrdU^{+}/NG2^{+}$ cells was significantly different from all the other proliferating cell populations (*$p<0.05$, one-way ANOVA followed by a Tukey's multiple comparisons test; $n=3$ confocal planes/islet, 5 islets/mouse, 3 mice/genotype). Scale bars, 20 μm (**a**) and 10 μm (**b**)

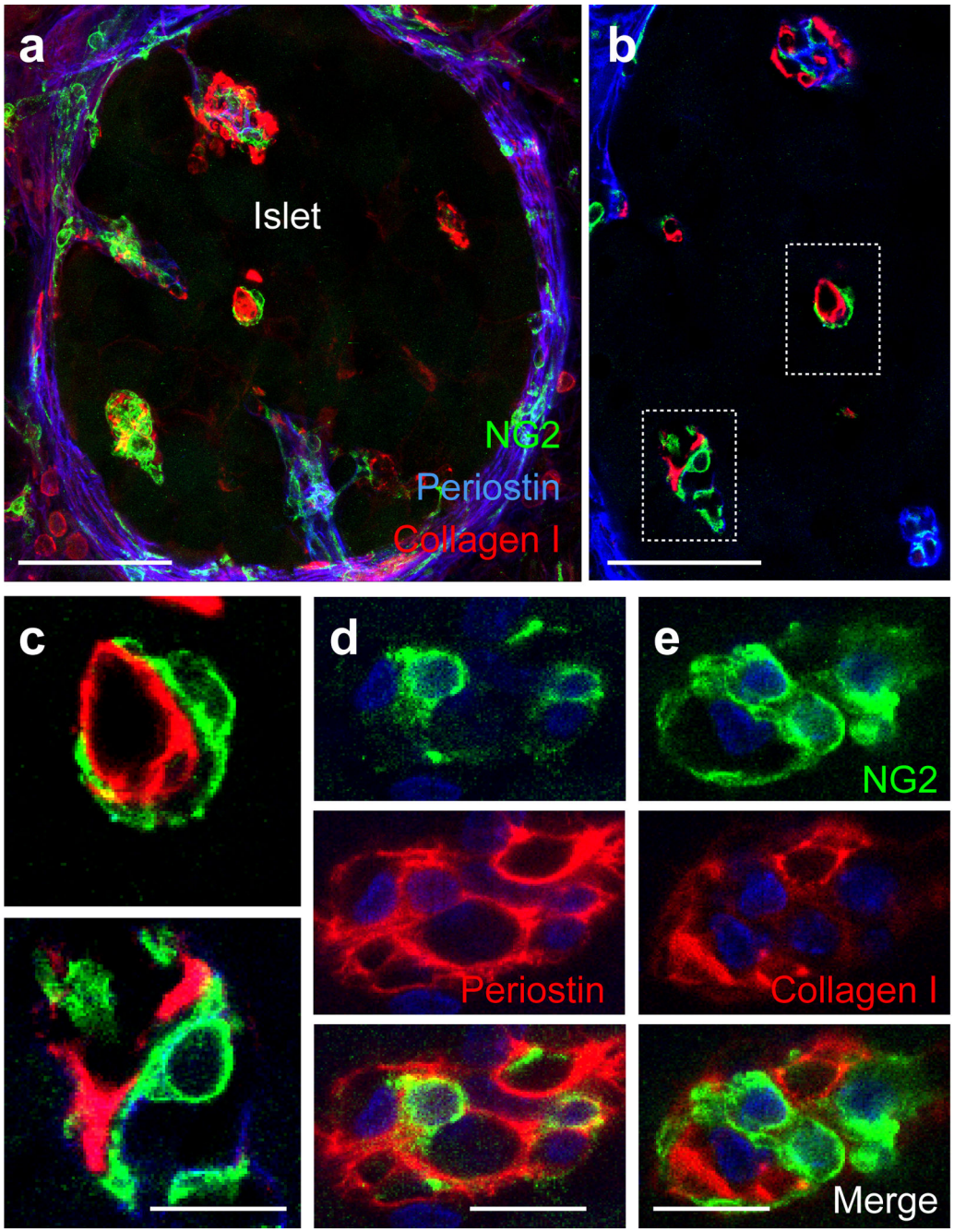

Fig. 4.

Pericytes associate with collagen type I and express periostin in *AktTg* islets. (**a**) Representative maximal projection of confocal images of an *AktTg* islet showing pericytes (NG2, green) in the vicinity of collagen type I (red) and the matricellular protein and myofibroblast marker periostin (blue). (**b**, **c**) Representative confocal images of islet pericytes (green) in an *AktTg* islet in close association with collagen type I (red). (**c**) Zoomed images of regions within dashed boxes shown in (**b**). (**d**, **e**) Representative confocal images of islet pericytes (NG2, green) and periostin (red, **d**) or collagen I immunostaining

(red, **e**). Merged images are shown underneath. These images are representative of 5 islets/mouse, 3 mice/genotype. Scale bars, 20 μm (**a**, **b**) and 10 μm (**c**–**e**)

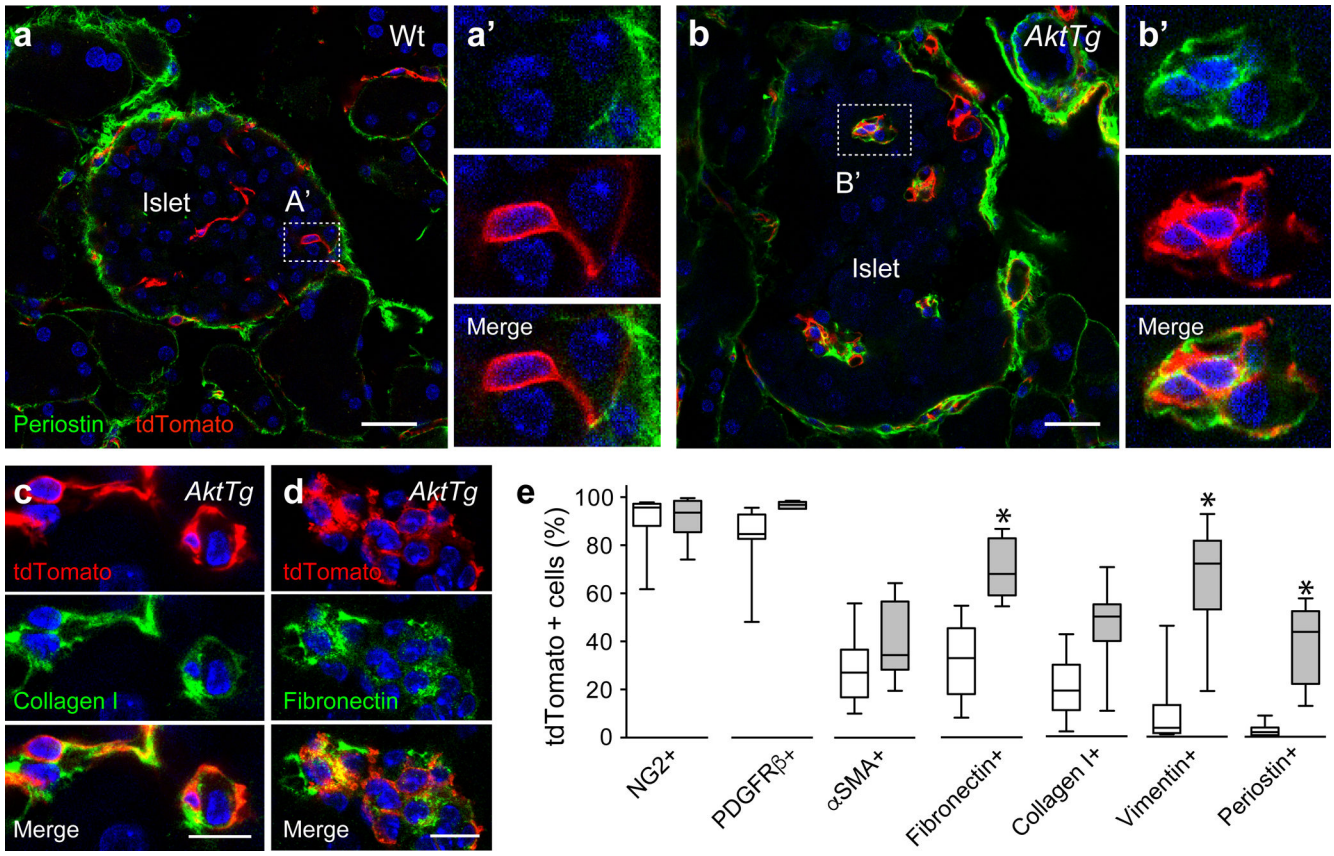

Fig. 5.

A subset of pericytes in *AktTg* islets differentiates into myofibroblasts. (**a**, **b**) Representative confocal images of an NG2-tdTomato wild-type islet (WT, **a**) and NG2-tdTomato-*AktTg* islet (*AktTg*, **b**) showing tdTomato-labelled pericytes and periostin immunostaining (green). Cell nuclei are shown in blue. (**a′** and **b′**) Higher magnification images of regions within dashed boxes. In wild-type islets, periostin is present in the interface between endocrine/exocrine tissue but not expressed by pericytes, while tdTomato-labelled pericytes in *AktTg* islets express periostin.

(**c**, **d**) Representative confocal images of regions in islets from NG2-tdTomato-*AktTg* mice showing tdTomato-labelled pericytes and collagen type I (green, **c**) and fibronectin immunostaining (green, **d**). Cell nuclei are shown in blue. tdTomato-labelled pericytes synthesising collagen I and fibronectin can be seen, as well as accumulation of these ECM proteins in their extracellular space. (**e**) Quantification of the fraction of tdTomato-positive cells that express the pericytic markers NG2, PDGFRβ and αSMA, ECM proteins fibronectin and collagen type I, and (myo)fibroblast markers vimentin and periostin in wild-type (white) and NG2-tdTomato-*AktTg* mice (grey). *$p<0.05$ (unpaired *t* test; $n=3$ confocal planes/islet, 5 islets/mouse, 2 mice/genotype). Scale bars, 20 μm (**a**, **b**) and 10 μm (**c**, **d**).

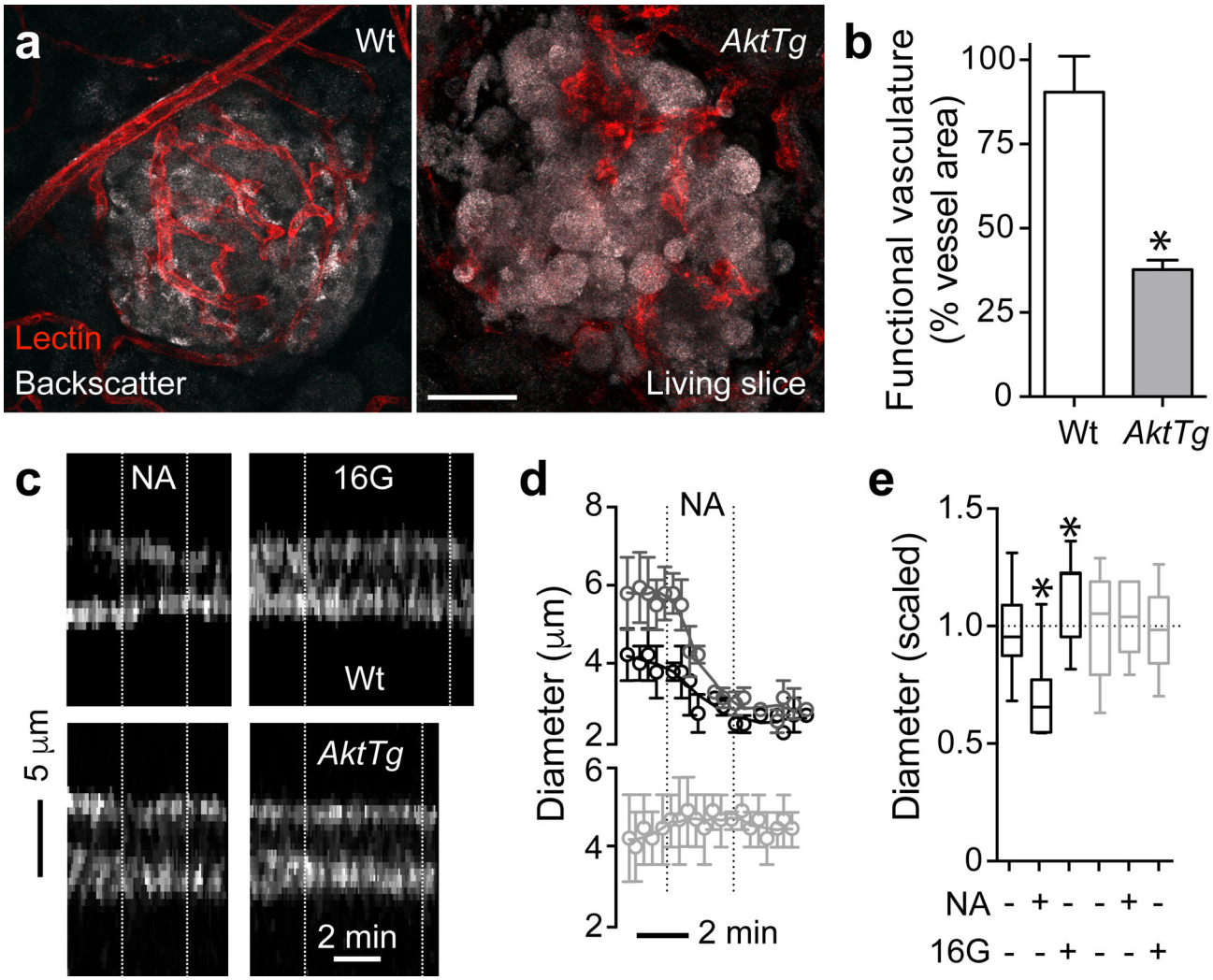

Fig. 6.

Impaired vascular perfusion and microvessel responses in *AktTg* islets ex vivo. (**a**) Representative maximal projections of confocal images of islets in living pancreatic slices from wild-type (WT) and *AktTg* mice. Blood vessels were labelled with an intravascular injection of fluorescent *Lycopersicon esculentum* lectin (red) 10 min before euthanising the animals. Endocrine cells in the islet can be visualised because of their higher backscatter signal (grey). Scale bar, 50 µm. (**b**) Quantification of the area of blood vessels that were labelled upon lectin injection (functional vasculature) as percentage of total islet vessel area. *$p<0.05$ (unpaired *t* test). (**c**) Temporal projections of line scans perpendicular to the vessel axis showing temporal patterns of changes in vessel diameter (see Methods). Capillary borders can be seen in white. Vertical white dashed lines indicate when the stimuli were present. Stimuli used were noradrenaline (NA; 20 µmol/l in 3 mmol/l glucose) and high glucose (16G; 16 mmol/l glucose). Noradrenaline induced a strong constriction of the wild-type islet capillary and high glucose dilated it. *AktTg* capillaries did not respond to the stimuli applied. (**d**) Traces of responses as in (**c**) show the mean change in vessel diameter induced by noradrenaline application (black symbols, capillaries in wild-type islets; dark

grey symbols, wild-type arterioles; light grey symbols, capillaries in *AktTg* islets; n=3–4 vessels per group). Vertical dotted lines indicate the time noradrenaline is present. (**e**) Quantification of changes induced by noradrenaline and high glucose in capillary diameter based on temporal projections as shown in (**c**). Black bars (wild-type) and grey bars (*AktTg*). Values were scaled to the initial diameter (before drug application, 3 mmol/l glucose). Only ~ 20% of islet capillaries responded upon stimulation. *p<0.05 (one-sample t test using as theoretical mean the value of 1 as diameter values were scaled to the initial diameter, indicated with the horizontal dashed line; n=3–4 vessels per group, 3 slices/mouse, 3 mice/genotype)